ACS SENSORS

pubs.acs.org/acssensors
Article

Develop Tandem Tension Sensor to Gauge Integrin-Transmitted Molecular Forces

Gopal Niraula,[#] Arghajit Pyne,[#] and Xuefeng Wang*

Cite This: *ACS Sens.* 2024, 9, 3660−3670
Read Online

ABSTRACT: DNA-based tension sensors have innovated the imaging and calibration of mechanosensitive receptor-transmitted molecular forces, such as integrin tensions. However, these sensors mainly serve as binary reporters, only indicating if molecular forces exceed one predefined threshold. Here, we have developed tandem tension sensor (TTS), which comprises two consecutive force-sensing units, each with unique force detection thresholds and distinct fluorescence spectra, thereby enabling the quantification of molecular forces with dual reference levels. With TTS, we revealed that vinculin is not required for transmitting integrin tensions at approximately 10 pN (piconewtons) but is essential for elevating integrin tensions beyond 20 pN in focal adhesions (FAs). Such high tensions have emerged during the early stage of FA formation. TTS also successfully detected changes in integrin tensions in response to disrupted actin formation, inhibited myosin activity, and tuned substrate elasticity. We also applied TTS to examine integrin tensions in platelets and revealed two force regimes, with integrin tensions surpassing 20 pN at cell central regions and 13−20 pN integrin tensions at the cell edge. Overall, TTS, especially the construct consisting of a hairpin DNA (13 pN opening force) and a shearing DNA (20 pN opening force), stands as a valuable tool for the quantification of receptor-transmitted molecular forces within living cells.

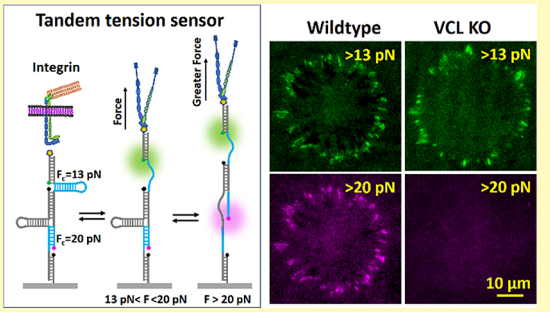

KEYWORDS: *shearing DNA, integrin tension, tension sensor, focal adhesion, vinculin*

Cells employ forces transmitted by mechanosensitive receptors within the cell membrane to orchestrate a diverse array of cellular and physiological activities.[1−3] These encompass vital functions such as cell adhesion,[4] migration,[5] embryogenesis,[6] cancer metastasis,[7] and immune activation.[8] In the field of cell mechanobiology, there is a keen pursuit of techniques for visualizing and quantifying these molecular forces. In the past decade, DNA has surfaced as a remarkably viable biomaterial for fabricating tension sensors due to its extensively documented mechanical attributes[9] and its adaptability for molecular synthesis and engineering.[10,11] DNA has been first applied to evaluate integrin tensions in live cells in 2013,[12] in which DNAs in unzipping, shear and intermediate configurations have been adopted to calibrate integrin tensions at different levels. Later, hairpin DNAs,[13,14] dsDNA (double-stranded DNA),[15,16] and shearing DNAs (reversible dsDNA in a shearing configuration)[17,18] have been adopted as the constructs of reversible or irreversible tension sensors. These tension sensors and associated microscopies have substantially improved the resolution,[16,19] sensitivity, and dynamic range of integrin tension visualization and calibration.

Although DNA-based tension sensors have demonstrated tremendous success for visualizing integrin tensions with high spatial resolution, previous sensors have primarily operated as binary probes, reporting if the force is larger than a predefined threshold. As a result, these sensors lack the capability of quantifying the local molecular force level. Although multiplexing tension sensors with different force thresholds have been practiced,[14,20] the nonidentical DNA structures of the multiplexed tension sensors would cause a bias due to the different accessibilities to the receptors, as one force sensor may be more sterically favorable than the other for the receptors to bind, leading to biased classification of force levels. Even if the multiplexed tension sensors share identical DNA conformations but exhibit different critical forces tuned by the GC content (the ratio of GC pairs to the total number of pairs), their accessibilities to cell membrane receptors may still vary. This is because the GC content influences the spontaneous opening rates of DNA structures,[21] potentially altering the distance between sensor ligands and the receptors. Variations in local densities of multiplexed tension sensors can introduce an additional source of bias. To overcome these biases, one effective approach is to link multiple force-reporting units in series, which share a single ligand molecule. This design ensures

Received: April 1, 2024
Revised: June 11, 2024
Accepted: June 27, 2024
Published: July 5, 2024

https://doi.org/10.1021/acssensors.4c00756
ACS Sens. 2024, 9, 3660−3670

that interconnected force-reporting units experience the exact same molecular tension transmitted by a cell receptor. Note that this strategy has been previously adopted in at least two research works. The You Lab linked two DNA hairpins to report the cadherin-transmitted forces between cells.[22] However, DNA hairpins typically exhibit unzipping forces in the range of 5−13 pN that are generally lower than integrin tensions that are capable of rupturing dsDNA in a shear configuration, which requires tens of piconewtons of force.[12,17] Therefore, interconnecting two DNA hairpins is not sufficient to quantify integrin tensions in the broad force range. We previously developed a ratiometric tension sensor with two linked dsDNAs, but this sensor is irreversible and only qualitatively responds to integrin tensions at different force levels.[23]

In this work, we developed tandem tension sensors (TTSs) in which two DNA-based force-sensing units are linked in series. Always under the same molecule force, these units have different opening forces and report the force in separate fluorescence spectra. By rational design, we synthesized TTS_5^{13} consisting of two hairpin DNAs and TTS_{13}^{20} consisting of one hairpin DNA and one shearing DNA. The superscript and subscript of the TTS are the two critical forces in unit of piconewtons. We validated their functionality using integrin tensions in FAs and in platelets, alongside vinculin knockout (VinKO) and several other approaches perturbing the generation and transmission of integrin tensions within cells. The results demonstrate that TTS_{13}^{20} effectively distinguishes various levels of integrin tensions in focal adhesions (FAs) and platelets, whereas TTS_5^{13} is not sensitive to these tension disparity. This suggests that TTS, comprising a hairpin DNA and a shearing DNA, has a dynamic range that aligns well with the range of integrin tensions in live cells.

MATERIALS AND METHODS

Cell Culture. HeLa cell lines were used as the cell models for TTS validation and integrin tension study in this work. Wild-type and vinculin knockout HeLa cell lines were purchased from American Type Culture Collection (CCL-2, ATCC) and Abcam (ab265580), respectively. Dulbecco's modified Eagle's medium (DMEM, 30−2002, ATCC) with high glucose supplemented with 10% fetal bovine serum (FBS, 30−2020, ATCC) and 1× penicillin-streptomycin (15140−122, Gibco) was used for cell culture of both HeLa cell lines (wild-type and vinculin knockout). HeLa cells were passaged every 72 h using the standard cell culture and passaging procedure, which can be found in the ATCC Web site.

TTS Construction. All DNAs are customized and purchased from Integrated DNA Technologies. The sequences and modifications are listed below. The detailed molecular structures are depicted in SFigures 1 and 2.

DNA sequences for TTS_5^{13}

DNA 1: /5ThioMC6-D/CCC ACC AGC GAC GCC CGG/3Cy3Sp/

DNA 1: /RGDfK/CCC ACC AGC GAC GCC CGG/3Cy3Sp/ (After RGDfK conjugation)

DNA 2: /5Atto647NN/TCG CGG CGA CCT CAG CAC TTT GTA TAA ATG TTTT CAT TTA TAC TTT CCG GGC GTC GCT GGT GGG

DNA 3: /5BHQ_2/GTG CTG AGG TCG CCG CGA TTT CGC GCG CGC TTTT GCG CGC GCG TTT AGC GCC ACG TAG CCC AGC

DNA 4: /5BiotinTEG/GCT GGG CTA CGT GGC GCT/3BHQ_2/

DNA sequences for TTS_{13}^{20}

DNA 1: /5ThioMC6-D/CCC ACC AGC GAC GCC CGG/3Cy3Sp/

DNA 1: /RGDfK/CCC ACC AGC GAC GCC CGG/3Cy3Sp/ (After RGDfK conjugation)

DNA 5: /5Atto647NN/TGG TCG TGC CTC TTT TCG CGG CGA CCT CAG CAC TTT CGCGCGCGC TTTT GCGCGCGCG TTT CCG GGC GTC GCT GGT GGG

DNA 6: /5BHQ_2/GTG CTG AGG TCG CCG CGA TTT GTA TAA ATG TTTT CAT TTA TAC TTT GAG GCA CGA CCT TTT AGC GCC ACG TAG CCC AGC

DNA 4: /5BiotinTEG/GCT GGG CTA CGT GGC GCT/3BHQ_2/

In DNA 1 strand, /5ThioMC6-D/represents a thiol modification used for conjugation with RGD peptide. /BHQ_2/is the Black Hole Quencher 2. DNA 1 was conjugated with a peptide ligand RGDfK before DNA hybridization. The conjugation of DNA 1 with RGDfK produces/RGDfK/CCC ACC AGC GAC GCC CGG/3Cy3Sp/. Briefly, the conjugation was conducted as follows:

> Step I: 10 μL solution of 50 mM TCEP solution (77720, Thermo Scientific) +50 mM EDTA in PBS (phosphate-buffered saline) at pH 7.4 was prepared. The mixture of TCEP and EDTA solution was used to deprotect the thiol group on the DNA and makes it accessible for thiol-maleimide reaction. The obtained 10 μL mixed solution was added to 20 μL × 1 mM thiol-DNA-Cy3 (DNA 1) in PBS and incubated for 30 min at room temperature.
>
> Step II: Next, 10 mg of RGD-NH_2 (PCI-3696-PI, Biosynth) was dissolved in 200 μL of ultrapure water. The RGD-NH_2 solution was added to 2 mg of solid sulfo-SMCC (A39268, Thermo Fisher Scientific) in a tube dipped in an ultrasonicator for quick dissolving and mixing. Afterwards, 22 μL 10× PBS was added to the mixture. This mixture was incubated for 15 min at room temperature.
>
> Step III: The DNA 1 solution (obtained from Step I) and RGD solution (obtained from Step II) were then mixed and incubated for 1 h at room temperature and then overnight at 4 °C. After this step, the majority of DNA (>90% according to our experience) should be conjugated with RGD. The RGD-DNA was purified by ethanol precipitation to remove unreacted RGD, SMCC and TCEP. Optionally, RGD-DNA purity can be examined with acrylamide gel electrophoresis which separates RGD-DNA and unconjugated DNA to two visible bands. RGD-DNA is in the lagging band which can be cut off, minced to small pieces, and soaked in PBS to further purify RGD-DNA. The RGD-DNA reconstituted in PBS can be stored at −20 °C for long-term storage. No noticeable degradation was observed after one year according to our experience.
>
> Step IV: Finally, TTS_5^{13} was assembled by hybridizing the RGD-DNA1 and DNA2, DNA3, DNA 4 at molar ratio DNA1:DNA2:DNA3:DNA4 = 1.3:1.2:1.1:1 with a final concentration of 10 μM in PBS. TTS_{13}^{20} was assembled by hybridizing the RGD-DNA1 and DNA5, DNA6, DNA 4 at molar ratio DNA1:DNA5:DNA6:DNA4 = 1.3:1.2:1.1:1 with a final concentration of 10 μM in PBS. The obtained TTS solutions were annealed by heating to 90 °C and cooling it back to room temperature. These obtained TTS can be stored in a freezer for more than a year without noticeable quality degradation.

TTS Immobilization on Glass-Bottomed Petri Dishes. The substrates for cell assays were glass-bottomed Petri dishes (D35−14−1.5-N, Cellvis) which support cell imaging with a 100 × oil lens. In our study, we immobilized TTS adopting the biotin-neutravidin chemistry to bind the sensor onto glass surfaces:

Step I: A solution of 100 μg/mL BSA-biotin (biotin-conjugated bovine serum albumin, A8549, Sigma-Aldrich, USA) and 2 μg/mL FN (fibronectin, 1918-FN, R&D System) in PBS buffer was added onto the well of a glass-bottomed Petri dish and incubated for 15 min at 4 °C. BSA and FN both can physically adsorb on the glass surface, and FN was used to facilitate cell adhesion. The surface was washed with cold PBS three times.

https://doi.org/10.1021/acssensors.4c00756
ACS Sens. 2024, 9, 3660−3670

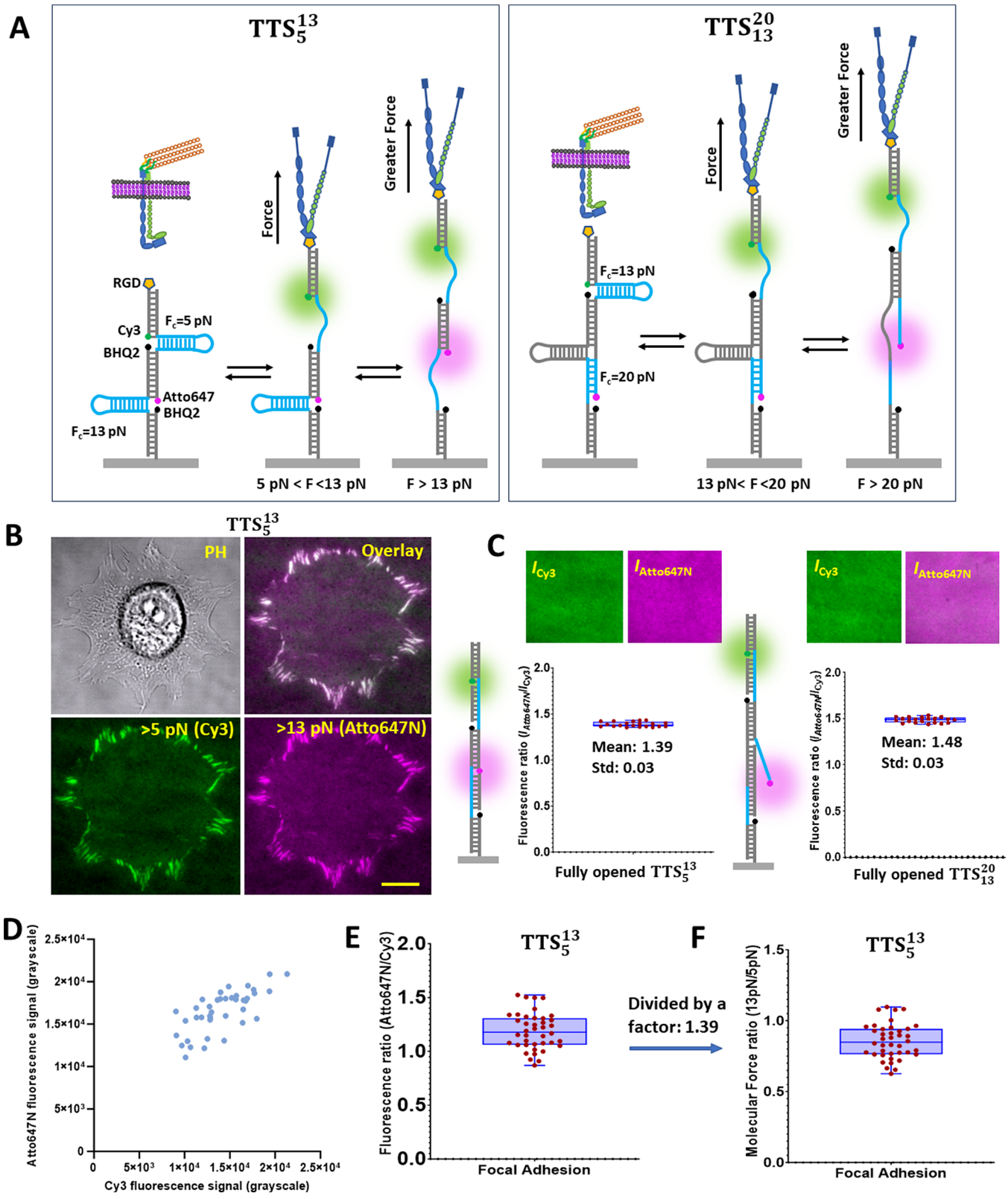

Figure 1. Construction and principle of TTS. (A) Schematics of TTS$_5^{13}$ and TTS$_{13}^{20}$. A molecular force higher than 5 pN would activate Cy3 of a TTS$_5^{13}$ construct, and a molecular force higher than 13 pN would activate both Cy3 and Atto647N. (B) Typical TTS force map, with Cy3 fluorescence reporting >5 pN integrin tensions and Atto647N reporting >13 pN integrin tensions. Scale bar: 10 μm. (C) Conversion factors were obtained to convert Atto647N-Cy3 fluorescence ratios to molecular force ratios (>13 pN/ >5 pN). TTSs were fully opened by complementary ssDNAs. The molecular ratio of two opened force-sensing domains is 1:1, and fluorescence ratios are 1.39 and 1.48 for TTS$_5^{13}$ and TTS$_{13}^{20}$, respectively. (D) Fluorescence intensities in both channels were calculated for 40 individual FAs, which were collected from four cells in one experiment. (E) Fluorescence ratios for individual FAs. (F) Molecular force ratios for individual FAs were obtained by dividing fluorescence ratios by 1.39.

https://doi.org/10.1021/acssensors.4c00756
ACS Sens. 2024, 9, 3660−3670

Step II: The washed surface was incubated with a solution of 50 μg/mL neutravidin (31000, Thermo Fisher Scientific) in PBS for 15 min at 4 °C and washed with cold PBS three times.

Step III: The surface was incubated with a solution of 100 nM TTS in PBS for 15 min at 4 °C and washed with PBS three times. The surface is ready for cell plating and further experiments.

TTS Immobilization on the PDMS Surface. In order to investigate whether cells sense elasticity via stress sensing and whether substrate rigidity impacts integrin molecular tension in cells, polydimethylsiloxane (PDMS) samples were prepared with different values of base:cross-linker ratio. PDMS is biocompatible and its mechanical properties are tunable. PDMS substrates with Young's modulus ranging from 1.704 MPa and 12 kPa were prepared by changing the base:cross-linker ratio from 10:1 and 50:1. The obtained stiffness in respective base:cross-linker ratio was previously calibrated using atomic force microscopy (Bioscope catalyst AFM, Bruker corporation, details given in later section). Elastomer base and cross-linker (04019862, SYLGARD 184 silicone elastomer base and curing agent kit) were combined thoroughly with a spatula in a 1.5 mL microcentrifuge tube. A 2 μL droplet of each mixture was sandwiched between two glass coverslips and kept for 10 min before separation. The two coverslips coated with PDMS mixture were kept to rest for 30 min so that the PDMS coating becomes uniform on the surfaces. Next, the coverslips were cured at 70 °C overnight on a hot plate. The coverslips were then removed from the hot plate and cooled down slowly. The ready-for-use PDMS coverslip was mounted onto an empty bottom Petri dish by an UV light-activated glue. The process of TTS immobilization on these surfaces was identical to that on regular glass surfaces.

HeLa Cell Detaching and Plating on to TTS Surfaces. First, cell culture medium was removed from Petri dish and the cells were rinsed with mild cell detaching solution [recipe: 100 mL of 10 × HBSS + 10 mL of 1 M HEPES + 10 mL of 7.5% sodium bicarbonate +2.4 mL of 500 mM EDTA + 878 mL of ultrapure water, pH 7.4]. The cells were then incubated in 2 mL of detaching solution inside an incubator with 5% CO_2 for 5 min. Cells were then pipetted off gently from the Petri dish and transferred into a centrifuge tube and centrifuged for 3 min at 300g. The cell pellet was suspended with the culture medium and added onto a TTS glass surface. The sample was incubated in a cell incubator for 1 h or otherwise stated time before imaging.

Cell Transfection. HeLa cells were transfected with pGFP(c3)-vinculin (plasmid #30312, Addgene) and pGFP(c1)-talin 1 (plasmid #26724, Addgene). DNA transfection was performed in wild-type and vinculin knockout HeLa cells with Lipofectamine LTX (15338−030, Invitogen) in opti-MEM media (11058021, Gibco) according to manufacturer's instructions. Briefly, ∼2.5 μg plasmid was mixed with 5 μL of Lipofectamine LTX in 500 μL of opti-MEM culture media and incubated at room temperature for 25 min. The mixture was then added to HeLa cells at 70% confluency in a Petri dish. The transfection was allowed for 24 h before further experiments.

Inhibition Treatments. CK666 (Arp2/3 inhibitor) and SMIFH2 (formin inhibitor) at a final concentration of 100 μM were added to cell solution. The treated cells were plated onto TTS surfaces and incubated for 10, 30, and 60 min at 5% CO_2 and 37 °C prior to TTS imaging.

During Y-27632 treatment, cells were preincubated for 1 h to allow FAs to form. The cell sample was mounted on a microscope. After that, the cell medium was exchanged with medium spiked with 20 μM Y-27632 and the cells were further incubated for 20 min. TTS imaging was performed on the cells right after adding Y-27632.

Quantification and Statistical Analysis. Image processing and data analysis were performed using the software (NIS-element) provided with the microscope combined with the MatLab code. The algorithm for the analysis of TTS signals in FAs is detailed in SFigure 3. GraphPad, Prism 10, was used for graph plotting. P values in figures were obtained using an unpaired t test.

Calculating Standard Deviations of the Product of Two Independent Variables. For two independent variables, X and Y, each following a normal distribution with means μ and ν, and standard deviations σ and τ, respectively, the standard deviation of XY is calculated as

$$\mathrm{Std}(XY) = \sqrt{\sigma^2\tau^2 + \sigma^2\nu^2 + \tau^2\mu^2}$$

For example, the product of two variables, 86% ± 12% and 27% ± 14%, is accompanied by a standard deviation of $\sqrt{0.12^2 \times 0.14^2 + 0.12^2 \times 0.27^2 + 0.14^2 \times 0.86^2} = 0.12 = 13\%$.

RESULTS AND DISCUSSION

Construction of TTS. We designed two TTS constructs, TTS_5^{13} and TTS_{13}^{20} (Figure 1A), with the subscript and the superscript numbers representing the critical forces (F_c, unit of piconewtons, pN) required to unfold the two force-sensing units in one TTS construct. These critical forces have been calibrated by previous work.[14,24] Refer to the next section for detailed discussion. Each TTS was synthesized by hybridizing four DNA oligonucleotide strands. The DNA sequences and modifications for each TTS are listed in SFigures 1 and 2. For each TTS construct, there are six DNA modifications: an integrin peptide ligand, a Cy3 dye, an Atto 647N dye, two blackhole quenchers (BHQ2) and a biotin. The biotin tag is to enable the surface immobilization of the TTS on surfaces through the biotin-neutravidin interaction. A Cy3-quencher pair and an Atto647N-quencher pair are adopted to label the two force-sensing units in each TTS. The molecular force acting on a TTS construct is detected through the fluorescence of Cy3 and Atto647N. When the force surpasses the respective critical force of a force-sensing unit, it causes DNA unfolding and pulls the dye away from the quencher, hence freeing the dye from quenching. The dyes of Cy3 and Atto647N were selected for their fluorescence stability.

We designed the DNA structures to ensure that each DNA strand has no more than two modifications to reduce the complexity of DNA synthesis. In both TTS constructs, the quenchers are positioned on the DNA strands closer to the substrate than the strands with the paired dyes. This design ensures that the quenchers, not the dyes, remain on the substrate if some TTS molecules spontaneously dissociate or become ruptured by ultrahigh integrin tensions, therefore eliminating the potential nonspecific fluorescence signal during TTS applications.

Critical Forces Required To Activate the Force-Sensing Units in the TTS Constructs. TTS_5^{13} was constructed by interconnecting two hairpin DNAs and tested to determine whether the critical force range of hairpin DNAs matches with the force range of integrin tensions in live cells. 5 pN and 13 pN were selected for constructing TTS_5^{13} as they represent the two extremes of critical unzipping forces for opening hairpin DNAs, which are determined by the GC content in the DNAs. We constructed TTS_{13}^{20} by adopting a hairpin DNA (13 pN critical force) and an 11-bp (base pair) shearing DNA (dsDNA in a shearing configuration) as force-sensing units. The critical force of 11-bp shearing DNA was previously found to represent a threshold value of integrin tensions required for cell adhesion but not sufficient for FA formation.[12]

Multiple research groups have conducted calibrations on the critical forces that dissociate hairpin DNAs and shearing DNAs, thereby aiding in the development of DNA-based tension sensors. The two force-sensing units of TTS_5^{13} are hairpin DNAs whose critical forces are determined by the GC content, with 22% GC content corresponding to 5 pN critical force and 100% GC content corresponding to 13 pN critical force, which were previously calibrated by the method of biomembrane force probe.[14] The calibrated critical force of a hairpin DNA represents a force level at which the hairpin DNA has equal probabilities of being at the folded state or the unfolded state.

https://doi.org/10.1021/acssensors.4c00756
ACS Sens. 2024, 9, 3660−3670

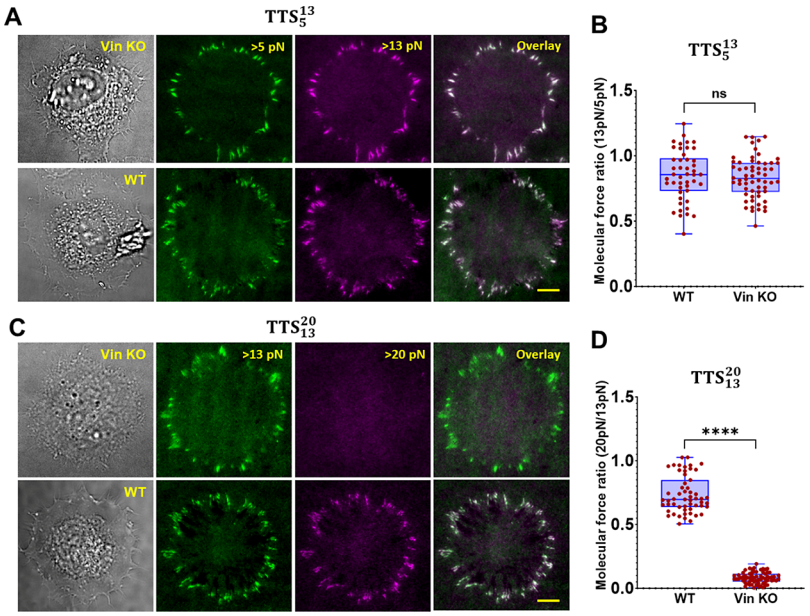

Figure 2. TTS calibrated integrin tensions in FAs of wild-type cells and vinculin knockout cells. (A) Integrin tension signals in WT HeLa cells and VinKO HeLa cells reported by TTS_5^{13}. Scale bar: 10 μm. (B) Molecular force ratios ($\frac{>13\text{ pN}}{>5\text{ pN}}$) of WT and VinKO cells. There is no significant difference between the two groups of ratios (P value = 0.64). 46 and 60 FAs were analyzed for the two groups, respectively. (C) Integrin tension signals reported by TTS_{13}^{20}. Scale bar: 10 μm. (D) Force molecule ratios ($\frac{>20\text{ pN}}{>13\text{ pN}}$) are 0.73 ± 0.14 and 0.08 ± 0.04 for WT and VinKO cells, respectively. This assay has been repeated for three times. 55 and 67 FAs in WT and VinKO cells, respectively, were pooled from three separate experiments. P values are <0.0001. Both P values were evaluated by using an unpaired Student t test.

The construct of TTS_{13}^{20} consists of one hairpin DNA and one 11-bp shearing DNA. The latter is coupled with an additional hairpin DNA to enable the reversible unfolding and refolding of the shearing DNA (Figure 1A). The unfolding force of an 11-bp reversible shearing DNA (60−70% GC content), characterized as the mean force rupturing the 11-bp reversible shearing DNA under a force loading rate of 1 pN/s, was recently calibrated by two groups using magnetic tweezers. The Liu group obtained a result of 45 pN at 22 °C[17] and the Yan group obtained a result of 20 pN at 37 °C.[24] Because all cell experiments in this work have been performed at 37 °C, and the reversible shearing DNA in TTS_{13}^{20} shares a similar conformation to that in ref 24, we adopted "20 pN" as the critical force of the 11-bp shearing DNA in this work. Note that a higher critical force of shearing DNA can be achieved by using longer DNA strand. For example, 15-bp shearing DNA has a critical force of "35 pN" as shown in ref 24. Therefore, TTS with higher critical forces can be constructed accordingly if needed.

Although we adopted the term "critical forces (F_c)" to denote all the force levels activating the force-sensing units in the TTS constructs, the reversible shearing DNA, consisting of a dsDNA (double-stranded DNA) and a hairpin DNA in TTS_{13}^{20}, has unique force-dependent kinetics which is different from that of a hairpin DNA. In a nutshell, the reversible shearing DNA is prone to unfolding when sustaining a force at the level of the dsDNA shearing force, but it is not folded back until the force becomes lower than the unzipping force of the coupled hairpin DNA, hence exhibiting a strong hysteresis in the force-dependent kinetics.[17] In this consideration, the 20 pN force-sensing unit in TTS_{13}^{20} may not be a real-time sensor reporting a current force level, and may have a memory that records past experience of a high-level force, until the current force is low enough to allow the refolding of the shearing DNA, thereby resetting its force-sensing ability. TTS_{13}^{20} can be regarded as a real-time tension sensor if the detected force is known to be a constant force with binary states (on or off) or a monotonically increasing force.

Demonstration of TTS Application. First, we demonstrated the application of TTS using TTS_5^{13} as an example. Figure 1B shows a HeLa cell plated on a glass surface coated with TTS_5^{13}. The coating concentration is 100 nM, which is expected to produce a surface density of TTS at ~1000/μm^2.[16] After incubation for 1 h, HeLa cells generated integrin tensions in streak patterns reported by both Cy3 and Atto647N signals, contributed by integrins in FAs. We verified that Cy3 and Atto647N fluorescence channels have no crosstalk in our experimental setup. The fluorescence signals suggested that both DNA hairpins in the TTS_5^{13} respond to integrin tensions. The ratio of Atto647N-Cy3 fluorescence intensities was calculated for individual FAs using the algorithm demonstrated in SFigure 3. To obtain the molecular ratio of two force-sensing units at the unfolded states (denoted as molecular force ratio), we prepared the versions of TTS_5^{13} and TTS_{13}^{20} with all force-sensing units fully opened by complementary DNAs hybridizing to the force-sensing units (Figure 1C). These complementary DNAs are detailed in SFigures 1 and 2. Because both force-sensing units in a TTS construct are fully unfolded, the molecular ratio of these two units at the unfolded states is 1:1. The Atto647N-Cy3 fluorescence ratios of fully extended TTS_5^{13} and TTS_{13}^{20} were obtained to be 1.39 and 1.48 (Figure 1C), respectively. These two numbers are used as conversion factors that convert fluorescence ratios of TTS signals to molecular force ratios in FAs. For example, the Atto647N-Cy3 fluorescence ratios within individual FAs (Figure 1D,E) were converted to 13 pN/5 pN molecular force ratios (Figure 1F), representing the ratios between integrin tensions above 13 pN and integrin tensions above 5 pN. The average 13 pN/5 pN

https://doi.org/10.1021/acssensors.4c00756
ACS Sens. 2024, 9, 3660−3670

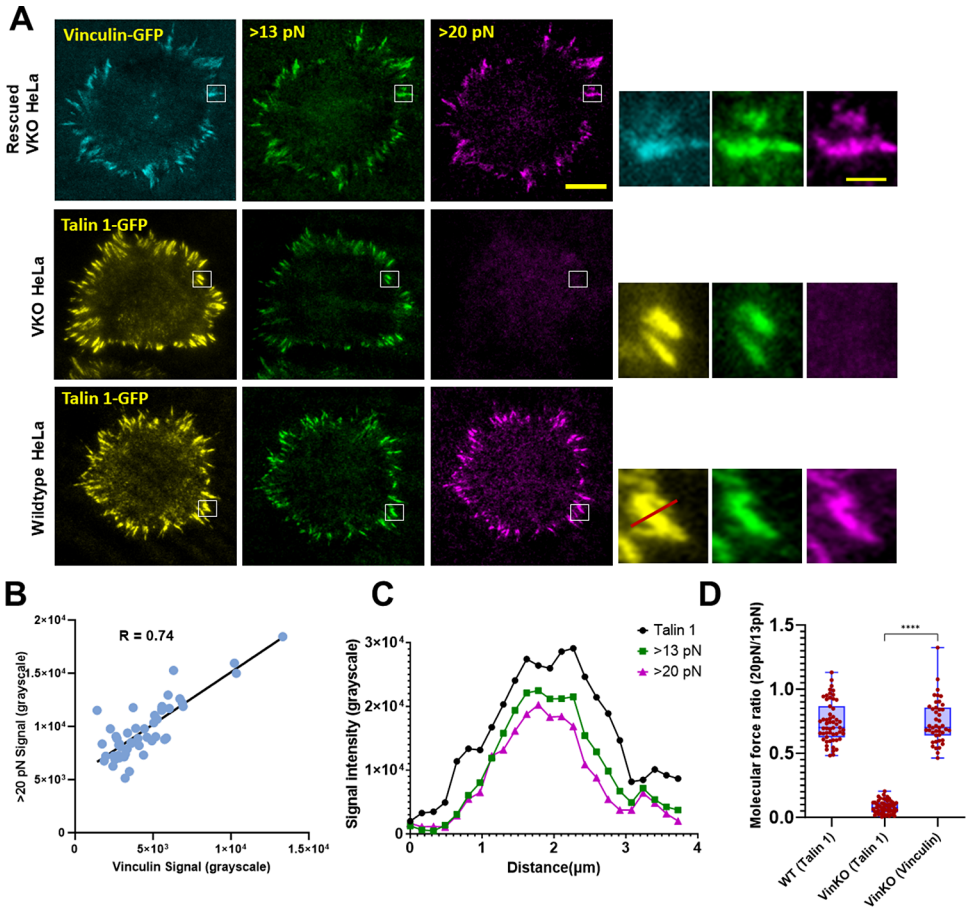

Figure 3. Vinculin expression by cell transfection restored >20 pN integrin tensions. (A) WT and VinKO cells were transfected to express vinculin-GFP or talin 1-GFP. Scale = 10 μm (2 μm in the zoom-in images). (B) Fluorescence intensity of vinculin-GFP is positively correlated with that of >20 pN force signal. (C) Line profiles of talin 1, >13 and >20 pN integrin tensions. Talin 1 is colocalized with integrin tension signals. (D) Integrin tension signals reported by TTS_{13}^{20}. Vinculin expression restored >20 pN integrin tensions, but talin 1 expression did not. The *P* value was evaluated by using an unpaired Student *t* test. 55 FAs pooled from three separate experiments were analyzed for each group of cells.

force ratio shown in Figure 1F is 0.86 ± 0.12, suggesting that 86% of all integrin tensions above 5 pN also exceed 13 pN.

We also demonstrated the performance of TTS_{13}^{20} in assessing integrin tensions in FAs and compared it to multiplexed single-threshold tension sensors, which consist of a hairpin tension sensor with a critical force of 13 pN and a shearing DNA tension sensor with a critical force of 20 pN as shown in SFigure 4A. These two tension sensors were mixed and coated on a surface at equal densities. HeLa cells were plated on the surfaces coated with TTS_{13}^{20} and multiplexed tension sensors, respectively. The average 20 pN/13 pN molecular force ratio shown in SFigure 4B is 0.75 ± 0.13, suggesting that 75% of all integrin tensions above 13 pN in FAs also exceed 20 pN, while the average 20 pN/13 pN molecular force ratio reported by multiplexed tension sensors is 0.55 ± 16. The significant difference between the two molecular force ratios indicates that multiplexed tension sensors cannot replace TTS in accurately reporting the force profile of integrin tensions. The lower molecular force ratio reported by multiplexed tension sensors could be due to the bulkier structure of the shearing DNA tension sensor (20 pN critical force) compared to the hairpin DNA tension sensor (13 pN critical force), potentially reducing its accessibility to integrins and causing a lower 20 pN/13 pN molecular force ratio.

Vinculin Is Critical for Generating Integrin Tensions above 20 pN in FAs. We tested the functionalities of TTSs using VinKO and WT HeLa cells. Vinculin is a mechanosensitive FA protein acting as a key regulator binding with talin and F-actin, connecting cells to the matrix and transmitting tension.[25] In addition, it also regulates the cell spreading and tension levels in FAs.[26,27] We applied TTS_5^{13} and TTS_{13}^{20} to assess the altered force levels of integrin tensions in VinKO cells. VinKO and WT HeLa cells were plated on TTS_5^{13} and TTS_{13}^{20} surfaces, respectively, as shown in Figure 2A,C. Data analysis shows that the 13 pN/5 pN force ratios generated by WT and VinKO cells are 0.86 ± 0.19 and 0.84 ± 0.19, respectively, showing insignificant difference (*P* value = 0.635, unpaired *t* test) between the two cell lines (Figure 2B). In contrast, on TTS_{13}^{20} surfaces, the 20pN/13pN force ratios generated by WT and VinKO cells are drastically different, with values of 0.73 ± 0.14 generated by WT cells and 0.08 ± 0.04 generated by VinKO cells (Figure 2D). The results suggest that 73% of all integrin tensions above 13 pN also exceed 20 pN in WT cells, while only 8% of such tensions exceed 20 pN if vinculin is knocked out.

The TTS_{13}^{20} data revealed that integrin tensions in FAs readily exceeded 20 pN, and vinculin is critical for elevating integrin tensions to this high level. Meanwhile, vinculin is not required for bringing integrin tensions above the level of 13 pN. We speculate that vinculin elevates integrin tension level by stabilizing the connection between talin and actin network. Talin is the important adaptor protein connecting integrins to actin network,[28] transmitting actomyosin force to integrins[29−31] and initiating inside-out integrin activation[32,33] through the

https://doi.org/10.1021/acssensors.4c00756
ACS Sens. 2024, 9, 3660−3670

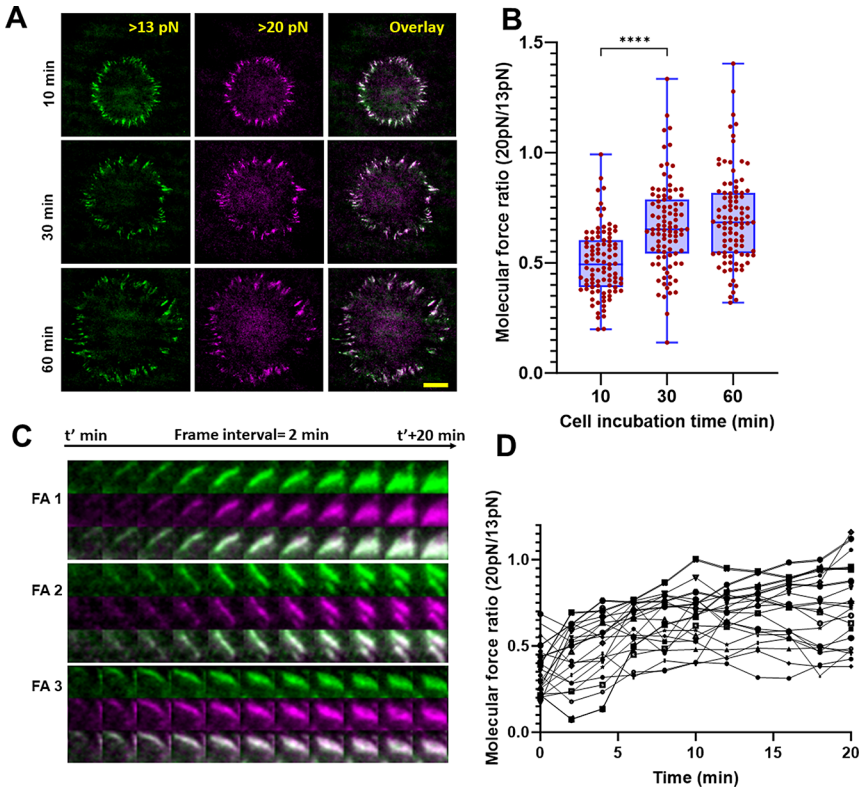

Figure 4. Molecular force ratios in FAs increase over the course of FA lifetimes. (A) HeLa cells incubated on TTS_{13}^{20} surfaces for 10, 30, and 60 min, respectively. Scale = 10 μm. (B) Molecular force ratios in FAs plotted against cell incubation times. (C) Force signals in single FAs during the course of FA life times. Refer to supplementary Movie 1. (D) Time trace of 20 pN/13 pN molecular force ratios in individual FAs.

integrin-talin-actin linkage. While the integrin-talin bond has been reported to be stabilized by kindlin,[34] the talin-actin connection could be reinforced by vinculin which binds to both talin and actin.[35] A recent work investigated the mechanical stability of vinculin-talin bonds,[36] reporting a bond lifetime in the order of seconds under a pulling force 15−25 pN, which is sufficient to transmit actomyosin-generated force to unfold the 20 pN force-sensing unit in TTS_{13}^{20}. In the absence of reinforcement from vinculin, a talin-actin bond might rupture before the integrin tension reaches 20 pN, or it may only persist for a brief period when sustaining a >20 pN force, insufficient to trigger the activation of the 20 pN force-sensing unit.

Vinculin Transfection in VinKO Cells Restored >20 pN Integrin Tensions. To further confirm that vinculin is the pivotal protein responsible for raising integrin tensions beyond 20 pN, we conducted transfections in VinKO cells to induce the expression of vinculin-GFP (green fluorescent protein). The transfected cells were incubated on the TTS_{13}^{20} surface for 1 h prior to imaging. Vinculin and TTS_{13}^{20} signals were then coimaged as shown in Figure 3A. Indeed, vinculin expression in VinKO cells restored high-level integrin tensions (>20 pN) in FAs. In addition, the vinculin expression level is also positively correlated with >20 pN integrin tension signal as shown in Figure 3B. To rule out the possibility that cell transfection or GFP expression induced >20 pN integrin tensions in vinculin-transfected VinKO cells, we transfected VinKO cells to express talin 1-GFP and found that this transfection did not restore >20 pN force signals in VinKO cells (which endogenously express talin). By talin transfection, we also observed that talin and >13 pN force signal are colocalized exceptionally well, as shown in the subimages in Figure 3A,C, affirming the important role of talin in transmitting integrin tensions. Overall, the transfection of vinculin into VinKO cells successfully restored >20 pN integrin tensions (Figure 3D), demonstrating that vinculin is the critical protein elevating integrin tensions beyond 20 pN.

20 pN/13 pN Force Ratio in FAs Increases Gradually by the Time of FA Formation. In the field of cell mechanobiology, an intriguing question concerns the force profile of integrin tensions in FAs during their initial formation stage. Using TTS_{13}^{20}, we explored the temporal dynamics of integrin tension level in FAs. First, WT HeLa cells were incubated on TTS_{13}^{20} surfaces for 10, 30, and 60 min prior to imaging (Figure 4A), producing 0.50 ± 0.15, 0.67 ± 0.20, and 0.70 ± 0.20 20 pN/13 pN force ratios, respectively. Next, we performed time trace imaging of TTS_{13}^{20} signal in live cells and tracked individual FAs from initial formation to a mature state. As shown in the supplementary Movie 1 and Figure 4C, in a WT cell plated on a TTS_{13}^{20} surface, FAs were formed with a turnover time of ∼20 min. We tracked a number of FAs and calculated the 20 pN/13 pN force ratios as shown in Figure 4D. The TTS signals of FAs were synchronized by treating the moment of TTS signal appearance as the time zero of an FA formation. The real-time TTS monitoring also exhibits a global increase of molecular force ratio by FA formation time, from 0.37 ± 0.15 at time zero to 0.74 ± 024. Overall, these experiments revealed significant 20 pN/13 pN force ratios even with 10 min cell incubation time or during the initial FA formation, suggesting that integrin tensions in FAs readily exceed 20 pN at the early stage of FA formation. The results also suggest the possibility that the portion of high-level integrin tensions (>20 pN) in FAs increases by time.

Despite scrutinizing data thoroughly, we observed no FAs exclusively generating a force signal greater than 13 pN but not exceeding 20 pN in WT cells, suggesting that a subpopulation of integrin tensions in FAs have already exceed 20 pN once the FAs

https://doi.org/10.1021/acssensors.4c00756
ACS Sens. 2024, 9, 3660−3670

are formed. We speculate that talin and vinculin recruitment may occur concomitantly in wild-type cells. This finding aligns with a recent publication, demonstrating the concurrent emergence of vinculin-GFP signals and integrin tension in cells.[37]

TTS_{13}^{20} Signals in FAs Respond to the Disruption of Actomyosin and Varied Substrate Stiffness. Previous studies have shown that both actin polymerization and myosin contraction contribute to integrin-transmitted forces in cells.[38−40] To test if TTS can report altered integrin tension levels with the perturbed actin polymerization and myosin contraction, we treated WT HeLa cells with Arp2/3 inhibitor CK666, which blocks actin filament branching, and formin inhibitor SMIFH2, which inhibits formin-mediated actin linear nucleation and growth.[41] The result shows that CK666 treatment did not have significant influence over the 20 pN/13 pN force ratios in FAs (Figure 5A,B), with values of 0.66 ± 0.19 and 0.67 ± 0.17 for the control group and the CK666-treated one, respectively. However, SMIFH2 treatment reduced the force ratio in FAs to 0.50 ± 0.15. These results suggest that Arp2/3-mediated actin branching has insignificant role, but formin-mediated actin linear nucleation is important for transmitting high-level integrin tensions. This observation aligns with a previous study showing that formin-mediated actin polymerization, but not Arp2/3-mediated actin branching, is essential for generating cytoskeletal forces on integrins.[42]

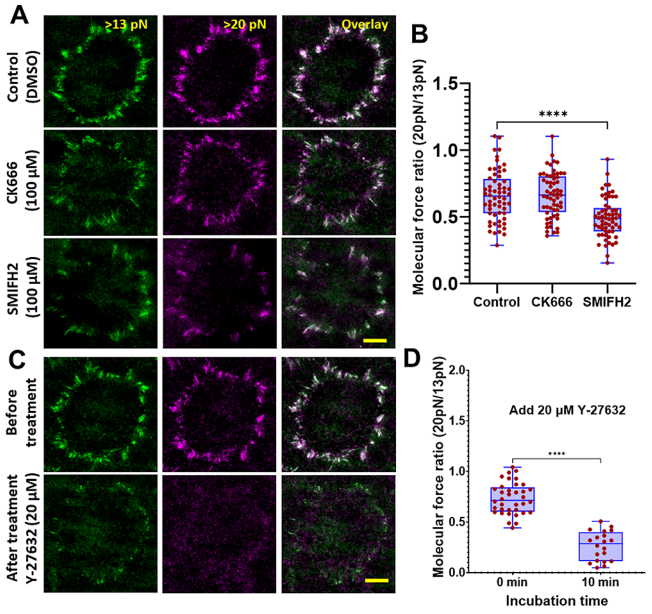

Figure 5. Actin polymerization and myosin II activity contribute to the 20 pN/13 pN molecular force ratios in FAs. (A) Force signals of TTS_{13}^{20} in HeLa cells with the treatment of CK666 inhibiting Arp2/3, or SMIFH2 inhibiting formin. Scale = 10 μm. (B) Molecular force ratios of TTS_{13}^{20} with the inhibition of Arp2/3 or formin. 60 FAs pooled from three separate experiments were analyzed for each group of cells. (C) Force signals of TTS_{13}^{20} of a HeLa cell before and after the treatment of Y-27632, a ROCK inhibitor. (D) Molecular force ratio of TTS_{13}^{20}. 36 and 20 FAs were analyzed for time points of 0 and 10 min, respectively. All P values were evaluated by using an unpaired Student t test.

Next, cells were treated with 20 μM Y-27632 that inhibits myosin II through the Rho-associated protein kinase (ROCK) pathway. While Y-27632 clearly reduced the TTS_{13}^{20} signal intensities in both fluorescence channels, the result also shows that the force ratio was reduced from 0.74 ± 0.15 to 0.26 ± 0.14. Taken together, the results suggest that the integrin tension level decreases if actomyosin in cells is perturbed. However, unlike vinculin knockout, none of these treatment completely abolished >20 pN integrin tensions while retaining >13 pN integrin tensions.

Integrin Tension Level in FAs Responds to Substrate Stiffness. One significant aspect of cell mechanotransduction is the capacity of cells detecting and responding to changes in matrix rigidity,[43,44] which has been shown to affect many cellular functions including cell adhesion, migration, and differentiation.[45−48] Because integrins are pivotal in cell mechanotransduction, we tested if TTS reports the potential change of integrin tension levels on elastic substrates. HeLa cells were plated on TTS_{13}^{20}-coated glass and polydimethylsiloxane (PDMS) surfaces with elastic modulus (E) of >1 GPa, 1.7 MPa and 12 kPa, respectively. The elastic modulus of PDMS substrates were previously calibrated.[23] The cells were incubated for 60 min prior to imaging (Figure 6A). Results show that molecular force ratios are 0.69 ± 0.20 and 0.71 ± 0.18 on the glass surface and the PDMS surface with E = 1.7 MPa, respectively, showing no significant difference. However, the molecular force ratio was reduced to 0.59 ± 0.18 on the PDMS surface with E = 12 kPa (Figure 6B), suggesting that integrin tension level in FAs reacted to the substrate rigidity, and TTS_{13}^{20} detected this change. Nevertheless, the alteration in molecular force ratio is surprisingly marginal across the tested substrate elasticities (GPa to 12 kPa), and high-level integrin tensions are consistently generated in FAs. A similar outcome was also reported in a recent publication, where tension sensors immobilized to hydrogels were employed to investigate integrin tensions.[18]

TTS_{13}^{20} Revealed Two Force Regimes of Integrin Tensions in Platelets. Platelets are small blood cells playing pivotal roles in blood coagulation. Integrins in platelets transmit tensions to orchestrate platelet activation, adhesion, and contraction. Previously, dsDNA-based tension sensors[15] and hairpin DNA-based tension sensors[49] have been applied to visualize integrin tensions in platelets. Here, we applied TTS_S^{13} and TTS_{13}^{20} to evaluate the force level of integrin tensions in human platelets.

As shown in Figure 7, integrin tensions in platelets were generated in two distinct patterns: the ring-like pattern at the cell edge and the plaque-like pattern within platelets, consistent with the previous report.[49] Integrin tensions in both patterns produced fluorescent signals in the two force channels of the TTS_S^{13} surface, suggesting that integrin tensions in both patterns exceed 13 pN in platelets (Figure 7A). However, on the TTS_{13}^{20} surface, while integrin tensions in the plaque-like pattern are visible in the two force channels, integrin tensions in the ring-like region only activate 13 pN force-sensing unit, but not the 20 pN force-sensing unit (Figure 7B). These results revealed that integrin tensions in the ring-like pattern are below 20 pN in platelets, but integrin tensions in the plaque-like region can surpass 20 pN. This force disparity is solely reported by TTS_{13}^{20} and not by TTS_S^{13}, indicating that a combination of a hairpin DNA and a shearing DNA in TTS is required to gauge the force of integrin tensions in platelets.

CONCLUSIONS

Integrins within FAs consistently transmit tensions that are critical mechanical signals regulating cell mechanotransduction. Numerous lines of evidence have shown that integrin tensions

https://doi.org/10.1021/acssensors.4c00756
ACS Sens. 2024, 9, 3660−3670

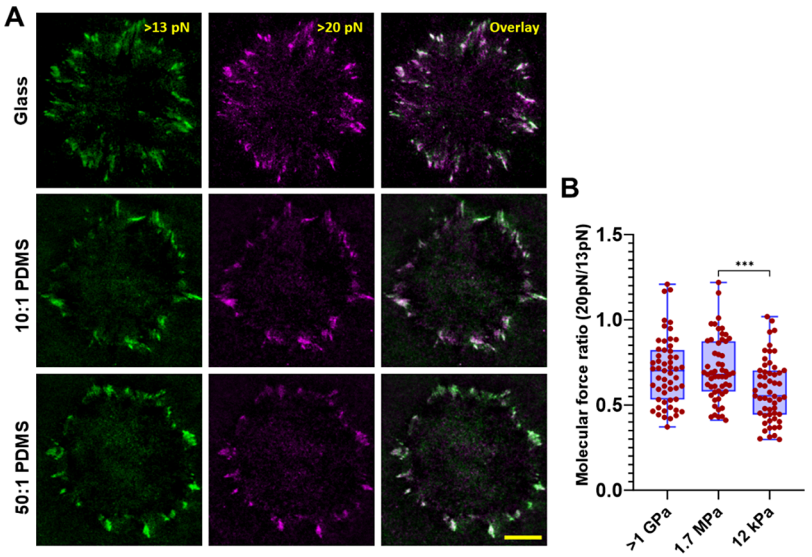

Figure 6. Molecular force ratio of TTS_{13}^{20} in FAs on elastic substrates. (A) HeLa cells incubated on TTS_{13}^{20}-coated glass and elastic PDMS surfaces. Scale = 10 μm. PDMS elastometer base and cross-linker ratios are 10:1 and 50:1, resulting in 1.7 MPa and 12 kPa Young's modulus. (B) Molecular force ratios in focal adhesions versus Young's modulus of substrates.

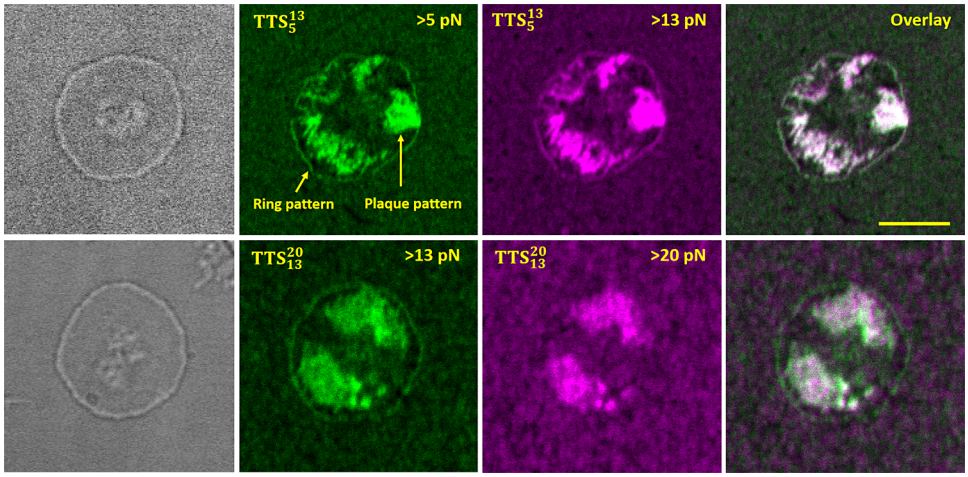

Figure 7. Integrin tensions in platelets exhibit two force regimes. Integrin tensions in platelets are produced in two patterns: a ring-shaped pattern located at the cell edge (indicated by yellow arrows) and a plaque-like pattern located within cell adhesion region. Integrin tensions in these patterns are visualized on TTS_5^{13} and TTS_{13}^{20} surfaces, respectively. Scale bar: 5 μm.

are active across a wide spectrum, ranging from a few piconewtons to tens of piconewtons.[12,17] To monitor integrin tensions within FAs, there is a growing need for molecular tension sensors that can quantitatively categorize these tensions across various molecular force levels in a broad dynamic range. To this end, we have designed the TTS, comprising two interconnected force-sensing components that assess the same molecular force using distinct detection thresholds. Two TTS constructs, TTS_5^{13} consisting of two hairpin DNAs with different GC contents and TTS_{13}^{20} consisting of a hairpin DNA and a shearing DNA, were developed by rational design and validated with VinKO cells, platelets, and common approaches perturbing cellular forces.

First, we tested TTS with HeLa cells, which readily form FAs. The results show that TTS_5^{13} yielded 0.86 ± 0.12 molecular force ratio, suggesting that, for all >5 pN integrin tensions, there are 14% ± 12% in the range of 5−13 pN and 86% ± 12% in the range of >13 pN. The TTS_{13}^{20} construct reported 0.73 ± 0.14 molecular ratio in live HeLa cells, suggesting that, for all >13 pN integrin tensions, there are approximately 27% ± 14% in the range of 13−20 pN and 73% ± 14% that exceeded 20 pN at some time points. Based on these results, we collectively estimate that, for all >5 pN integrin tensions, there is 14% ± 12% integrin tensions in the range of 5−13 pN, 86% × 27% = 23% (±13%) in the range of 13−20 pN and 86% × 73% = 63% (±15%) that exceeded 20 pN at some time points. The standard deviations of 13 and 15% were calculated using the method described in support information. These findings indicate a substantial portion of integrin tensions have exceeded 20 pN within FAs, implying that a prior study which reported a small fraction of integrin tensions exceeding 11 pN[50] may have underestimated the prevalence of high integrin tensions. TTS results also show that both 13 pN/5 pN and 20 pN/13 pN molecular force ratios are rather uniform inside individual FAs.

To further confirm TTS's ability of assessing mechanical forces, we utilized both VinKO and wild-type HeLa cells to investigate how TTS responds to potential alterations in integrin tensions resulting from the vinculin knockout. In VinKO cells,

https://doi.org/10.1021/acssensors.4c00756
ACS Sens. 2024, 9, 3660−3670

the TTS_5^{13} signal had little change in terms of force signal intensity or molecular force ratio. However, TTS_{13}^{20} result shows that nearly all >20 pN integrin tensions are abolished and >13 pN integrin tensions are retained with vinculin knockout. The >20 pN integrin tensions and the 20 pN/13 pN molecular force ratio were restored by transfecting VinKO cells to express vinculin. This result not only validates that TTS_{13}^{20} effectively responded to alterations in integrin tensions due to vinculin knockout but also strongly underscores the essential role of vinculin in elevating integrin tensions beyond 20 pN. This observation is consistent with several previous studies that have demonstrated the role of vinculin in increasing integrin tensions,[50−52] attesting to the functionality of TTS in assessing integrin tension levels. TTSs have also been shown to respond to changes in integrin tensions resulting from the inhibition of actomyosin and variations in substrate elasticities. Furthermore, we validated the performance of TTS_5^{13} and TTS_{13}^{20} with human platelets. The results show that platelets generate integrin tensions in two distinct force regions, with peripheral region transiting integrin tensions in 13−20 pN and the central region transmitting integrin tensions above 20 pN. The different force levels were only reported by TTS_{13}^{20}, which consists of a hairpin DNA and a shearing DNA, indicating that TTS consisting of two hairpin DNAs is insufficient to gauge integrin tensions in live cells. Overall, with the capability to quantify force levels of integrin tensions in real time and within live cells, TTS, especially the one consisting of a hairpin DNA and a shearing DNA, provides a valuable and convenient tool for investigating cell mechanotransduction, expanding our knowledge of how cells respond to mechanical stimuli.

■ ASSOCIATED CONTENT

Supporting Information

The Supporting Information is available free of charge at https://pubs.acs.org/doi/10.1021/acssensors.4c00756.

Molecular structures of TTS_5^{13} and TTS_{13}^{20}; MatLab algorithm; and comparison of TTS_{13}^{20} and multiplexed tension sensors in evaluating integrin tensions in FAs (PDF)

■ AUTHOR INFORMATION

Corresponding Author

Xuefeng Wang − *Research Division in Hoxworth Center, College of Medicine, University of Cincinnati, Cincinnati, Ohio 45219, United States;* orcid.org/0000-0002-3301-3196; Email: xuefeng.wang@uc.edu

Authors

Gopal Niraula − *Department of Physics and Astronomy, Iowa State University, Ames, Iowa 50011, United States*

Arghajit Pyne − *Research Division in Hoxworth Center, College of Medicine, University of Cincinnati, Cincinnati, Ohio 45219, United States*

Complete contact information is available at: https://pubs.acs.org/10.1021/acssensors.4c00756

Author Contributions

#G.N. and A.P. equally contributed to this work. X.W. conceived the concept, synthesized the tension sensors, and supervised the project. G.N. and A.P. performed experiments and obtained and analyzed data. G.N. and X.W. prepared the manuscript.

Notes

The authors declare no competing financial interest.

■ ACKNOWLEDGMENTS

This work was supported by National Institute of General Medical Sciences (1R35GM128747) and the startup fund provided by University of Cincinnati. We are grateful to the quality control team (Jenine Fields, Stacy Braun, Katheryn Boedecker, Sheryl Heeb, Lindsey O'Bannion, Desmond Taylor, Jennifer O'Connor, et al.) at Hoxworth blood center for providing the platelet samples.

■ REFERENCES

(1) Bershadsky, A. D.; Balaban, N. Q.; Geiger, B. Adhesion-Dependent Cell Mechanosensitivity. *Annual Review of Cell and Developmental Biology* **2003**, *19* (1), 677−695.

(2) Martino, F.; Perestrelo, A. R.; Vinarsky, V.; Pagliari, S.; Forte, G. Cellular Mechanotransduction: From Tension to Function. *Front. Physiol.* **2018**, *9*, 824.

(3) Chen, Y. F.; Ju, L. N.; Rushdi, M.; Ge, C. H.; Zhu, C. Receptor-mediated cell mechanosensing. *Mol. Biol. Cell* **2017**, *28* (23), 3134−3155.

(4) Bachmann, M.; Kukkurainen, S.; Hytönen, V. P.; Wehrle-haller, B. Cell Adhesion by Integrins. *Physiol Rev.* **2019**, *99* (4), 1655−1699.

(5) Trepat, X.; Wasserman, M. R.; Angelini, T. E.; Millet, E.; Weitz, D. A.; Butler, J. P.; Fredberg, J. J. Physical forces during collective cell migration. *Nat. Phys.* **2009**, *5* (6), 426−430.

(6) Sutlive, J.; Xiu, H. N.; Chen, Y. F.; Gou, K.; Xiong, F. Z.; Guo, M.; Chen, Z. Generation, Transmission, and Regulation of Mechanical Forces in Embryonic Morphogenesis. *Small* **2022**, *18* (6), No. e2103466, DOI: 10.1002/smll.202103466.

(7) Kumar, S.; Weaver, V. M. Mechanics, malignancy, and metastasis: The force journey of a tumor cell. *Cancer and Metastasis Reviews* **2009**, *28* (1−2), 113−127.

(8) Smith-garvin, J. E.; Koretzky, G. A.; Jordan, M. S. T Cell Activation. *Annu. Rev. Immunol.* **2009**, *27*, 591−619.

(9) Bustamante, C.; Bryant, Z.; Smith, S. B. Ten years of tension: single-molecule DNA mechanics. *Nature* **2003**, *421* (6921), 423−427.

(10) Roh, Y. H.; Ruiz, R. C. H.; Peng, S. M.; Lee, J. B.; Luo, D. Engineering DNA-based functional materials. *Chem. Soc. Rev.* **2011**, *40* (12), 5730−5744.

(11) Albrecht, C.; Blank, K.; Lalic-mülthaler, M.; Hirler, S.; Mai, T.; Gilbert, I.; Schiffmann, S.; Bayer, T.; Clausen-schaumann, H.; Gaub, H. E. DNA:: A programmable force sensor. *Science* **2003**, *301* (5631), 367−370.

(12) Wang, X.; Ha, T. Defining single molecular forces required to activate integrin and notch signaling. *Science* **2013**, *340* (6135), 991−994.

(13) Blakely, B. L.; Dumelin, C. E.; Trappmann, B.; Mcgregor, L. M.; Choi, C. K.; Anthony, P. C.; Duesterberg, V. K.; Baker, B. M.; Block, S. M.; Liu, D. R.; Chen, C. S. A DNA-based molecular probe for optically reporting cellular traction forces. *Nat. Methods* **2014**, *11* (12), 1229−1232.

(14) Zhang, Y.; Ge, C.; Zhu, C.; Salaita, K. DNA-based digital tension probes reveal integrin forces during early cell adhesion. *Nat. Commun.* **2014**, *5* (1), 5167.

(15) Wang, Y. L.; Levine, D. N.; Gannon, M.; Zhao, Y. C.; Sarkar, A.; Hoch, B.; Wang, X. F. Force-activatable biosensor enables single platelet force mapping directly by fluorescence imaging. *Biosens Bioelectron* **2018**, *100*, 192−200.

(16) Zhao, Y. C.; Pal, K.; Tu, Y.; Wang, X. F. Cellular Force Nanoscopy with 50 nm Resolution Based on Integrin Molecular Tension Imaging and Localization. *J. Am. Chem. Soc.* **2020**, *142* (15), 6930−6934.

(17) Li, H.; Zhang, C.; Hu, Y.; Liu, P.; Sun, F.; Chen, W.; Zhang, X.; Ma, J.; Wang, W.; Wang, L.; Wu, P.; Liu, Z. A reversible shearing DNA probe for visualizing mechanically strong receptors in living cells. *Nat. Cell Biol.* **2021**, *23* (6), 642−651.

(18) Wang, W. X.; Chen, W.; Wu, C. Y.; Zhang, C.; Feng, J. J.; Liu, P. X.; Hu, Y. R.; Li, H. Y.; Sun, F.; Jiang, K.; Zhang, X. H.; Liu, Z. Hydrogel-based molecular tension fluorescence microscopy for investigating receptor-mediated rigidity sensing. *Nat. Methods* **2023**, *20*, 1780−1789, DOI: 10.1038/s41592-023-02037-0.
(19) Brockman, J. M.; Su, H. Q.; Blanchard, A. T.; Duan, Y. X.; Meyer, T.; Quach, M. E.; Glazier, R.; Bazrafshan, A.; Bender, R. L.; Kellner, A. V.; Ogasawara, H.; Ma, R.; Schueder, F.; Petrich, B. G.; Jungmann, R.; Li, R. H.; Mattheyses, A. L.; Ke, Y. G.; Salaita, K. Live-cell super-resolved PAINT imaging of piconewton cellular traction forces. *Nat. Methods* **2020**, *17* (10), 1018−1024.
(20) Wang, Y. L.; Wang, X. F. Integrins outside focal adhesions transmit tensions during stable cell adhesion. *Sci. Rep.* **2016**, *6*, No. 36959.
(21) Chen, H.; Skylaris, C. K. Analysis of DNA interactions and GC content with energy decomposition in large-scale quantum mechanical calculations†. *Phys. Chem. Chem. Phys.* **2021**, *23* (14), 8891−8899.
(22) Zhao, B.; Li, N.; Xie, T.; Bagheri, Y.; Liang, C.; Keshri, P.; Sun, Y.; You, M. Quantifying tensile forces at cell−cell junctions with a DNA-based fluorescent probe. *Chemical Science* **2020**, *11* (32), 8558−8566.
(23) Sarkar, A.; Niraula, G.; Levine, D.; Zhao, Y.; Tu, Y.; Mollaeian, K.; Ren, J.; Que, L.; Wang, X. Development of a Ratiometric Tension Sensor Exclusively Responding to Integrin Tension Magnitude in Live Cells. *ACS Sensors* **2023**, *8*, 3701−3712.
(24) Liu, J. Z.; Le, S. M.; Yao, M. X.; Huang, W. M.; Tio, Z.; Zhou, Y.; Yan, J. Tension Gauge Tethers as Tension Threshold and Duration Sensors. *ACS Sensors* **2023**, *8* (2), 704−711.
(25) Hu, K.; Ji, L.; Applegate, K. T.; Danuser, G.; Waterman-storer, C. M. Differential transmission of actin motion within focal adhesions. *Science* **2007**, *315* (5808), 111−115.
(26) Alenghat, F. J.; Fabry, B.; Tsai, K. Y.; Goldmann, W. H.; Ingber, D. E. Analysis of cell mechanics in single vinculin-deficient cells using a magnetic tweezer. *Biochemical and biophysical research communications* **2000**, *277* (1), 93−99.
(27) Mierke, C. T.; Kollmannsberger, P.; Zitterbart, D. P.; Smith, J.; Fabry, B.; Goldmann, W. H. Mechano-coupling and regulation of contractility by the vinculin tail domain. *Biophys. J.* **2008**, *94* (2), 661−670.
(28) Giannone, G.; Jiang, G.; Sutton, D. H.; Critchley, D. R.; Sheetz, M. P. Talin1 is critical for force-dependent reinforcement of initial integrin−cytoskeleton bonds but not tyrosine kinase activation. *J. Cell Biol.* **2003**, *163* (2), 409−419.
(29) Austen, K.; Ringer, P.; Mehlich, A.; Chrostek-grashoff, A.; Kluger, C.; Klingner, C.; Sabass, B.; Zent, R.; Rief, M.; Grashoff, C. Extracellular rigidity sensing by talin isoform-specific mechanical linkages. *Nature cell biology* **2015**, *17* (12), 1597−1606.
(30) Kanchanawong, P.; Shtengel, G.; Pasapera, A. M.; Ramko, E. B.; Davidson, M. W.; Hess, H. F.; Waterman, C. M. Nanoscale architecture of integrin-based cell adhesions. *Nature* **2010**, *468* (7323), 580−584.
(31) Kumar, A.; Ouyang, M.; Van den dries, K.; Mcghee, E. J.; Tanaka, K.; Anderson, M. D.; Groisman, A.; Goult, B. T.; Anderson, K. I.; Schwartz, M. A. Talin tension sensor reveals novel features of focal adhesion force transmission and mechanosensitivity. *J. Cell Biol.* **2016**, *213* (3), 371−383.
(32) Calderwood, D. A.; Zent, R.; Grant, R.; Rees, D. J. G.; Hynes, R. O.; Ginsberg, M. H. The talin head domain binds to integrin β subunit cytoplasmic tails and regulates integrin activation. *J. Biol. Chem.* **1999**, *274* (40), 28071−28074.
(33) Goult, B. T.; Bouaouina, M.; Elliott, P. R.; Bate, N.; Patel, B.; Gingras, A. R.; Grossmann, J. G.; Roberts, G. C.; Calderwood, D. A.; Critchley, D. R. Structure of a double ubiquitin-like domain in the talin head: a role in integrin activation. *EMBO J.* **2010**, *29* (6), 1069−1080.
(34) Bodescu, M. A.; Aretz, J.; Grison, M.; Rief, M.; Faessler, R. Kindlin stabilizes the talin•integrin bond under mechanical load by generating an ideal bond. *Proc. Natl. Acad. Sci. U. S. A.* **2023**, *120* (26), No. e2218116120, DOI: 10.1073/pnas.2218116120.
(35) Bays, J. L.; Demali, K. A. Vinculin in cell-cell and cell-matrix adhesions. *Cell. Mol. Life Sci.* **2017**, *74* (16), 2999−3009.
(36) Le, S. M.; Yu, M.; Yan, J. Direct single-molecule quantification reveals unexpectedly high mechanical stability of vinculin-talin/α-catenin linkages. *Sci. Adv.* **2019**, *5* (12), No. eaav2720, DOI: 10.1126/sciadv.aav2720.
(37) Bender, R. L.; Ogasawara, H.; Kellner, A. V.; Velusamy, A.; Salaita, K. Unbreakable DNA tension probes show that cell adhesion receptors detect the molecular force-extension curve of their ligands. *bioRxiv* **2022**, DOI: 10.1101/2022.04.04.487040.
(38) Clarke, D. N.; Martin, A. C. Actin-based force generation and cell adhesion in tissue morphogenesis. *Curr. Biol.* **2021**, *31* (10), R667−R680.
(39) Harris, A. R.; Jreij, P.; Fletcher, D. A. Mechanotransduction by the actin cytoskeleton: converting mechanical stimuli into biochemical signals. *Annual review of biophysics* **2018**, *47*, 617−631.
(40) Vasioukhin, V.; Bauer, C.; Yin, M.; Fuchs, E. Directed actin polymerization is the driving force for epithelial cell−cell adhesion. *Cell* **2000**, *100* (2), 209−219.
(41) Courtemanche, N. Mechanisms of formin-mediated actin assembly and dynamics. *Biophysical reviews* **2018**, *10* (6), 1553−1569.
(42) Jo, M. H.; Li, J.; Jaumouillé, V.; Hao, Y.; Coppola, J.; Yan, J.; Waterman, C. M.; Springer, T. A.; Ha, T. Single-molecule characterization of subtype-specific β1 integrin mechanics. *Nat. Commun.* **2022**, *13* (1), 7471.
(43) Discher, D. E.; Janmey, P.; Wang, Y.-L Tissue cells feel and respond to the stiffness of their substrate. *Science* **2005**, *310* (5751), 1139−1143.
(44) Pelham, R. J., Jr; Wang, Y.-L. Cell locomotion and focal adhesions are regulated by substrate flexibility. *Proc. Natl. Acad. Sci. U. S. A.* **1997**, *94* (25), 13661−13665.
(45) Fu, J.; Wang, Y.-K.; Yang, M. T.; Desai, R. A.; Yu, X.; Liu, Z.; Chen, C. S. Mechanical regulation of cell function with geometrically modulated elastomeric substrates. *Nat. Methods* **2010**, *7* (9), 733−736.
(46) Geiger, B.; Spatz, J. P.; Bershadsky, A. D. Environmental sensing through focal adhesions. *Nat. Rev. Mol. Cell Biol.* **2009**, *10* (1), 21−33.
(47) Prager-khoutorsky, M.; Lichtenstein, A.; Krishnan, R.; Rajendran, K.; Mayo, A.; Kam, Z.; Geiger, B.; Bershadsky, A. D. Fibroblast polarization is a matrix-rigidity-dependent process controlled by focal adhesion mechanosensing. *Nature cell biology* **2011**, *13* (12), 1457−1465.
(48) Vogel, V.; Sheetz, M. Local force and geometry sensing regulate cell functions. *Nat. Rev. Mol. Cell Biol.* **2006**, *7* (4), 265−275.
(49) Zhang, Y.; Qiu, Y. Z.; Blanchard, A. T.; Chang, Y.; Brockman, J. M.; Ma, V. P. Y.; Lam, W. A.; Salaita, K. Platelet integrins exhibit anisotropic mechanosensing and harness piconewton forces to mediate platelet aggregation. *P Natl. Acad. Sci. USA* **2018**, *115* (2), 325−330.
(50) Tan, S. J.; Chang, A. C.; Anderson, S. M.; Miller, C. M.; Prahl, L. S.; Odde, D. J.; Dunn, A. R. Regulation and dynamics of force transmission at individual cell-matrix adhesion bonds. *Sci. Adv.* **2020**, *6* (20), No. eaax0317.
(51) Austin, J.; Tu, Y.; Pal, K.; Wang, X. F. Vinculin transmits high-level integrin tensions that are dispensable for focal adhesion formation. *Biophys. J.* **2023**, *122* (1), 156−167.
(52) Ma, R.; Rashid, S. A.; Velusamy, A.; Deal, B. R.; Chen, W. C.; Petrich, B.; Li, R. H.; Salaita, K. Molecular mechanocytometry using tension-activated cell tagging. *Nat. Methods* **2023**, *20*, 1666−1671.